Surface Modification of Mobile Composition of Matter (MCM)-41 Type Silica Nanoparticles for Potential Oral Mucosa Vaccine Delivery.

Muhammad Khairul Amin[1], Joshua S. Boateng[1*].

[1] School of Science, Faculty of Engineering and Science, University of Greenwich, Medway, Kent, ME4 4TB

[*]Corresponding Author

Email: J.S.Boateng@gre.ac.uk; joshboat40@gmail.com

Tel: +44 (0) 208 331 8980

Fax: +44 (0) 208 331 9805

Abstract

Development of mobile composition of matter (MCM)-41 silica nanoparticles faces challenges, e.g. surface charge properties, antigen loading efficiency, protecting from enzymes and harsh GIT environment and effective release at target mucosal site. We report the production and characterization of polymer and amine modified MCM-41 type silica nanoparticles for oral antigen delivery and with ovalbumin (OVA) as model antigen. Nanoparticles were characterized by dynamic light scattering (DLS), differential scanning calorimetry, X-ray diffraction, scanning electron microscopy (SEM), Brunauer-Emmett-Teller **(**BET), circular dichroism (CD), sodium dodecyl sulfate–polyacrylamide gel electrophoresis (SDS-PAGE), mucin binding, stability in simulated gastric fluid (SGF) and simulated intestinal fluid (SIF) and *in vitro* OVA release in SGF and SIF. Unmodified nanoparticles size 146nm increased to 175-321nm after modification while modified particles remained intact for more than 3 hrs in SGF and 96 hrs in SIF (DLS and SEM). Mucin binding proved PEG and chitosan modified nanoparticles as potential candidates for mucosal oral delivery. Both showed highest OVA encapsulation at 67% and 73%, and sustained OVA release in SIF (96 hrs) at 65% and 64% respectively. BET results showed that nanopores were not blocked during surface modification. CD and SDS-PAGE showed that OVA conformational structure did not change after release from nanoparticles.

Keywords: chitosan, nanocarrier, ovalbumin, mucoadhesive vaccine delivery, polyethylene glycol, silica surface modification.

1. Introduction

Since the discovery of MCM- mobile composition of matter (MCM)-41mesoporous silica nanoparticles (MSNs) in 1992, scientists have made tremendous efforts at exploring its potential application in biomedical research [1]. The delivery of specific protein into cells to influence cellular function requires a multifunctional cargo carrier which is able to encapsulate antigen and tailor it for targeting specific cells or tissues [2]. In this respect, silica nanoparticles have attracted considerable interest due to their biocompatibility, low toxicity, large surface area, pore volume, controlled release and stability in biological fluids. Another advantage of MSNs is the high internalization within various immune cells via endocytosis compared to other competing carriers, e.g. polymeric or synthetic organic materials [3]. However, several barriers have to be overcome to allow efficient antigen delivery because protein antigens are impermeable to cell membranes due to electrostatic repulsion and degradation or inactivation in body fluids [4]. Due to their structure and ability to protect encapsulated antigens from premature degradation in biological fluids, MSNs could be employed to increase efficiency of antigen delivery *in vivo* by avoiding antigenic protein denaturation [5] Protein encapsulation in MSNs is still challenging due to the small pore diameter (< 3nm) preventing protein molecules from entering the interior pores of the MSNs [6]. An alternative option is to design MSNs which would have large enough pores and internal surface area to allow protein molecules to be adsorbed and protected more effectively [7]. Research studies have shown that particles with size range of 50-200nm have achieved better uptake by endocytosis than particles with size greater 200nm [8].

MSNs can especially achieve higher endocytosis for intracellular antigen delivery, when they are functionalized with positively charged moieties such as amine groups, polyethylene glycol (PEG) and polyethyleneimine (PEI) [9]. These functional groups have been used to modify MSNs surface properties to achieve adjustable stimuli responsive delivery

systems based on environmental factors such as pH, enzymes, light and thermal (temperature) stability [10] as well as achieve higher protein encapsulation efficiency or higher binding capacity with nanoparticles [11].

To produce silica nanoparticles with suitable properties, sol-gel process has typically been used, specifically, MCM-41 type MSNs fabrication by soft templating method with two-dimensional hexagonal structure and pore sizes > 2nm. In this method, tetraethyl orthosilicate (TEOS) is used as a silica source, the cationic surfactant cetyltrimethylammonium bromide (CTAB) used as a soft template and an alkaline compound as a catalyst [12]. Generally, MCM-41 type MSNs have particle size less than 300nm, which has great potential for efficient immune cell internalization in antigen delivery research [13]. However, a major limitation of MCM-41 type MSNs is aggregation and various research studies have used different kinds of bases to catalyze the hydrolysis and condensation of TEOS to form colloidal complexes and modify their surface properties to prevent particle aggregation. The synthesis of amino functionalized dendrimer-like silica nanoparticles using sol-gel synthesis procedure, with TEOS as silica precursor, CTAB as a surfactant, ammonia as a catalyst, and 3-aminopropyltriethoxysilane (APTES) as functional modification agent in an ethyl-ether-water system was reported [14] and produced MSNs with particle size range of 200-700nm and pore sizes > 4nm.

To date, very few studies have focused on surface functionalization of MCM-41 nanoparticles to achieve optimum mucoadhesive performance for effective mucosal vaccine delivery. Therefore this study seeks to enhance high antigen encapsulation and minimize agglomeration properties due to their high surface area and large pore volume, modify the MCM-41 particle surface to provide a rigid framework and suitable protection of encapsulated antigen from the harsh GIT environment (acidic pH and presence of proteases). In addition, surface modified nanoparticles are expected to provide sustained release of

loaded antigen in the intestinal environment and reduce flocculation that can occur via non-specific binding of active functional groups on MCM-41 nanoparticles' surface. This study involves the synthesis of MSNs and investigation and comparison of the effect of surface modification using four different organic materials on nanoparticles properties. Specifically, the surfactant templating method was chosen to synthesize MSNs of approximate size ranging between 120 and 450nm. Hydrophobic MCM-41 nanoparticles were surface modified with four different materials: APTES, poly(methyl methacrylate) (PMMA), PEG, and chitosan to obtain partially hydrophobic, mucoadhesive and stable shells to promote sustained release of encapsulated model antigen. In addition, the effect of functionalization on the surface properties of the nanoparticles particularly their surface charge, hydrophilicity character, protein loading efficiency, protein release properties, stability in physiological fluid and formation of the protein corona that modulates their biological activity were investigated.

2. Materials and Method

Tetraethyl orthosilicate (TEOS, >99%, M.W. 208.33), cetyltrimethylammonium bromide [(CTAB), >99%, M.W. 364.45), sodium hydroxide (NaOH) ≥ 97.0% pellets, M.W. 40.00, 3-aminopropyl-triethoxysilane (APTES, > 98% M.W. 221.37), polyethylene glycol (PEG) M.W. 16000-24000, chitosan (75-85% deacetylated, M.W. 190,000-310,000), poly(methyl methacrylate-co-methacrylic acid) (PMMA, ratio 1: 0.016, M.W. 15000), OVA from chicken egg white (≥ 98%, M.W. 44287Da.), pepsin from porcine gastric mucosa,, mucin (0.5-1.5 % bound sialic acid) from porcine stomach, sodium chloride, acetic acid, sodium acetate, sodium dihydrogen phosphate, hydrochloric acid, maleic acid (≥ 99%, M.W. 116.07), were obtained from Sigma-Aldrich, (Gillingham, UK). Quick Start™ Bradford protein assay reagent was purchased from Bio Rad, (Watford, UK). All other reagents were of analytical grade.

2.1 Synthesis of MCM-41 nanoparticles

MCM-41 type silica nanoparticles were synthesized as previously reported [15] with slight modifications. The basic synthesis of MSNs was conducted by mixing the silica source, (TEOS) with the templating surfactant (CTAB) in ultrapure double distilled water. In a round bottom flask, 833mg of CTAB was dissolved in 100ml double distilled water, 1.5ml of 2M NaOH standard solution was added and the resulting solution was heated at 80°C for 30 min whilst being stirred vigorously. After that, 0.4ml of TEOS was added dropwise into the CTAB solution and stirred at 80°C for a further 2 hrs. After formation of a white cloudy suspension, the temperature was slowly reduced with continuous stirring (4 hrs) until the temperature was stabilized at room temperature. The white precipitate (MCM-41 nanoparticles) was collected by centrifugation at 20,000rpm and washed with methanol 3 times at the same rpm to remove excess surfactant. The collected sample (pellet) was designated as MCM-41 nanoparticles.

For amine surface modification, 2g of the MCM-41 was dispersed in 90ml deionized water and 10ml APTES was added dropwise into the resulting dispersion and stirred for 24 hrs under temperature-controlled water bath at 20°C. The formulation was then centrifuged and washed with methanol 3 times to remove surfactants and unbound APTES. For the PEG modification, 100mg of PEG was dissolved in 100ml of a 50:50 dioxane: water solution at room temperature and approximately 2g of MCM-41 MSNs dispersed in the PEG solution and stirred for 24 hrs. PEG has two reactive ends and one reactive end can be attached to the particle surface and limits the coupling process only to one end. For PMMA modification, MCM-41 MSN (2g) was dispersed in 90ml water and 10ml PMMA added dropwise and stirred at room temperature for 24 hrs. PMMA modified MCM-41 nanoparticles were collected by centrifugation at 20000rpm. After centrifugation, white solid particles (pellet) were deposited at the bottom of centrifuge tube which was recovered by discarding the supernatant. The collected pellet was washed three times with water by centrifugation as described before. For

chitosan modification 100mg chitosan was dissolved in 90ml acetic acid solution (1.0%) and 2g MCM-41 white particles dispersed in the chitosan solution and vigorously stirred for 24 hrs and then washed with water 3 times via centrifugation.

2.2 Protein encapsulation studies

OVA stock solution (0.5mg/mL) was prepared in phosphate buffer (pH 7.4). Plain MCM-41 and surface modified equivalents (2mg/mL) were sonicated (5 min) and dispersed in the same buffer. In a typical procedure, 0.5mg/ mL of the OVA stock solution was mixed with 2mg/ml of MCM-41, MCM-41 APTES, MCM-41-PMMA, MCM-41-PEG and MCM-41-chitosan suspensions and incubated in a water bath shaker (400rpm, 20 °C). After overnight incubation, protein-loaded particles (were collected by centrifugation (13 000 rpm, 30 min) and separated from the non-encapsulated (free) protein, which remained in the supernatant. The encapsulation efficiency (EE%) was determined by measuring the difference in concentration of the protein in the supernatant before and after loading. The concentration of protein was determined by Bradford assay using a standard calibration curve of OVA. The intrinsic fluorescence intensity and absorbance were measured using 96-well plate in a plate reader (Thermo Fisher multiskan, photometer). The standard curves were based on the absorbance of OVA within the concentration range of 0.1mg/ml to 3mg/ml. The calibration curves were based on the absorbance at 620 and 540, respectively, as a function of concentration. The EE (%) and loading capacity (LC) (%) were calculated as shown in equations 1 & 2.

$$\mathbf{EE}\ (\%) = \frac{\mathbf{total\ amount\ of\ OVA - free\ OVA\ in\ supernatent}}{\mathbf{total\ amount\ of\ OVA}} \times \mathbf{100} \qquad \mathbf{(1)}$$

$$\mathbf{LC}\ (\%) = \frac{\mathbf{total\ amount\ of\ OVA - free\ OVA\ in\ supernatent}}{\mathbf{Dried\ nanoparticles\ weight}} \times \mathbf{100} \qquad \mathbf{(2)}$$

2.3 In-vitro protein release study

To determine the amount of protein released from OVA loaded nanoparticles, the Bradford reagent (protein-specific dye, Coomassie brilliant blue) was used and analyzed with 96-well polystyrene plate as above and performed in triplicate. Freeze dried OVA loaded nanoparticle (5mg|) were dispersed in 0.01% sodium azide containing 2ml of SGF (pH 1.2) and SIF pH 6.8) and were incubated at 37°C in bath shaker with gentle stirring. At pre-determined time intervals over 24 hrs, 0.1ml aliquots of dissolution media were collected and replaced with same amount of fresh simulated fluid. The samples were analyzed with plate reader at an absorbance of 595nm and Bradford reagent standard were used according to manufacturer's instruction kit.

2.3 Characterization

2.3.1 Particle size and zeta potential evaluation using dynamic light scattering (DLS)

DLS was used to measure particle size, polydispersity index (PDI) and zeta potential with the help of a Zetasizer Nano-ZS90 (Malvern Instruments, UK) using disposable cuvette for size and PDI analysis. Zeta potential was measured using the Malvern Zetasizer with a reusable folded capillary zeta cell, (Malvern Model: DTS1070) by determining the electrophoretic mobility. The sample was measured in deionized water and adjusted to a conductivity of 50 S/cm with sodium chloride solution (0.9% w/v). The pH was 7.4 and the applied field strength was 20V/cm. The sample was properly diluted (1ml sample and 1ml deionized water) to achieve concentrations between 2 – 3 % w/w and scanned with constant refractive index viscosity and dielectric constant for all formulations at controlled temperature of 20°C. For each sample, 15 runs of 10 s were performed, with three repetitions for all the blank nanoparticles and protein loaded nanoparticles. The intensity of size distribution, the Z-average

diameter (Z-ave) and the PDI were obtained from the autocorrelation function using the "general purpose mode.

2.3.2 Morphology by scanning electron microscopy and scanning transmission electron microscopy

The morphology of MCM-41 nanoparticles was examined by scanning electron microscopy (SEM) (Hitachi SU8030) at operating voltage of 1kV. In this study 1kV was found harmless for MCM-41 nanoparticles observation. One drop of freshly prepared particles suspensions was deposited on SEM sample stub and left until air dried and the dried sample was chromium coated for 3 min. For scanning transmission electron microscopy (STEM) analysis, the sample was diluted (1:2) and stained with 2% (w/v) phosphotungstic acid for 30 s and placed on copper grids with films for observation. The dried specimens were examined at high resolution for morphological characteristics of the nanoparticles. Excess liquid was removed by using filter paper before observation on the STEM machine.

2.3.3 Attenuated total reflectance Fourier transform infrared (ATR-FTIR) spectroscopy

Infrared absorption spectra were obtained for both pure starting materials and the formulated nanoparticles at room temperature. Attenuated total reflectance (ATR)-FTIR (Perkin Elmer, Spectrum Two) spectra were performed in transmittance mode (%T) mode, with 32cm^{-1} resolution and scan speed of 0.2 over a wavelength range of 450–4000cm^{-1}. The samples were placed on ZnSe ATR crystal and maximum pressure was applied using a pressure clamp accessory to allow intimate contact between the samples and the ATR crystal. Different peaks in the IR spectrum were interpreted for different functional groups in the formulations.

2.3.4 X-ray diffraction (XRD)

X-ray diffraction was performed to investigate crystalline or amorphous nature of the formulated nanoparticles. The diffractograms were recorded with a Brucker AXS D8 Advance instrument using Cu-ka line as a source of radiation and operated at a voltage of 40keV and current of 35mA. Freeze dried formulated samples were measured in the range between 3º and 50º 2θ for 2 hrs and step size of 0.02º and scan speed of 0.5s/step.

2.3.5 Differential scanning calorimetry (DSC)

DSC analysis (Mettler Toledo 823e, Greifensee, Switzerland)) was performed to characterize the physical state of the starting materials, lyophilized plain MCM-41 nanoparticles, surface modified MCM-41 nanoparticles and protein loaded nanoparticles. About 3mg of accurately weighed sample was placed into aluminium pans with lids and analyzed at a scanning temperature range from 0°C to 300°C and heating rate of 10°C/min under dry nitrogen atmosphere. The initial temperature of 0°C was maintained with the help of liquid nitrogen.

2.3.6 Nanoparticles stability studies in SGF and SIF

MCM-41 surface modified nanoparticles were analyzed for colloidal stability in SGF and SIF and experiment performed by using previously reported method [16] with slight modification. The composition of SGF and SIF are provided in tables S1 and S2 (Supplementary data). Freeze dried MCM-41 nanoparticles was weighed (1mg/ml) into respective simulated fluid contained in a round shaped bottle and placed in shaking water bath (200rpm) at 37°C for 12 and 96 hrs in the SGF and SIF respectively. At time intervals of 30 mins, both fluids were sampled, and particles analyzed for size using Zetasizer and by SEM to investigate the effect of pH and ions on size and shape of protein loaded nanoparticles over time. Measuring the size distribution of the surface modified nanoparticles in different simulated biological fluids at different time points helped to monitor any nanoparticle aggregation as an indicator of colloidal

stability. Further, the withdrawn protein loaded MCM-41 nanoparticles suspension was passed through Millipore filter and the protein lost from the nanoparticles analyzed using Bradford assay as described above.

2.3.7 *In vitro* mucin binding of (MCM)-41 surface modified nanoparticles.

The mucoadhesive properties of MCM-41 nanoparticles were investigated as previously described [16], but with minor modification. Briefly, 0.5ml of mucin solution (0.5mg/ml) was mixed with 0.5ml of each surface modified MCM-41 nanoparticle suspension and incubated at 37°C in a shaking water bath for 2 hrs. After centrifugation at 16000rpm for 40 min, the supernatant was collected, and the amount of free mucin was measured using Bradford protein assay. The supernatant was incubated with Bradford reagent for 5 min in a 96 well plate, after which the absorbance (620nm) was measured with a plate reader (Multiskan FC Microplate Photometer, Thermo Fisher Scientific). Mucin concentration was calculated from a standard curve of mucin in concentration range from 0.1 to 1.0mg/ml. The amount of mucin binding with nanoparticles was determined using equation (1) mentioned above.

2.3.8 Circular dichroism analysis

Circular dichroism (CD) spectra were obtained using a Chirascan spectrophotometer (Applied Photophysics Limited) to examine the secondary structure of OVA during the release period. Spectra were collected at 20°C using a quartz cell (path length 0.05cm) and the wavelength range of 180-260nm and a resolution of 0.2nm with 2.25 second response time. Each spectrum represents an average of four consecutive scans. Noise reduction, blank solution subtraction and data analysis were performed using standard analysis and temperature/wavelength analysis program (Origin pro 8, USA)). OVA was extracted from samples after 96 hrs *in vitro* release study by centrifuging at 5000rpm before CD analysis and compared with native OVA.

2.3.9 Sodium dodecyl sulfate–polyacrylamide gel electrophoresis (SDS–PAGE) analysis

One dimensional SDS-PAGE analysis was performed on OVA released from the MCM-41 surface modified nanoparticles to determine primary structure after 96 hrs in SIF (pH 6.8). The gel (4-12%) was prepared by following a previously reported method [18]. Briefly, a separating gel prepared with 3.4ml deionized water, 2ml of 1.5M tris-HCl (pH 8.8), 2.4ml of 30% poly acrylamide, 100µl of 10% SDS, 100µl ammonium persulfate and 10µl of tetramethyl ethylenediamine was poured into the gel cassette (Bio-Rad). The whole assembly was left to stand for 15-20min to allow the gel to solidify and stacking gel was then poured on top of the separating gel and a 10-lane comb was added. Aliquots (20µl) of the OVA containing suspensions were mixed with similar volume of SDS loading buffer in a 1 ml centrifuge tube. The resulting mixture was then heated to 95 °C for 10 min in a heating block (DIGI-BLOCK^{TM}) to denature the disulfide bonds of the proteins and cooled to room temperature and centrifuged to remove any suspended solids. Tris-HCl, pH 6.8, 1mM ethylenediamine tetraacetic acid (EDTA), 2-mercaptoethanol and bromophenol blue mixture, served as tracking agent. 2-mercaptoethanol was the reducing agent and was responsible for breaking the disulfide bridges and denaturing the protein molecules. Aliquots (20µl) of the supernatant was then transferred on top of the gel in a Bio-Rad mini gel tank and both upper lower chambers were filled with SDS- running buffer. The gel run was performed at a constant voltage of 200V for 1 hour. The gel was stained with Coomassie blue staining solution and washed with 5% (v/v) acetic acid solution overnight and images captured by a BioDoc-It® Imaging System, (UVP, LLC, Upland, USA).

2.3.10 Brunauer-Emmett-Teller (BET) analysis

Freeze dried MCM-41 surface modified nanoparticles were investigated for pore volume, surface area and pore diameter by using BET (Micromeritics, Gemini VI) analysis. About 60mg of sample was placed in the glass cell and degassed at 45ºC for more than 36 hrs with high vacuum pressure to remove water and contaminants before surface area was measured. The surface area was calculated by BET theory using isotherm adsorption data at P/P0 from 0.0 to 0.3. Liquid nitrogen was used to cool the sample and maintained at a constant temperature of -196ºC.

2.3.11 Statistical analysis

All the quantitative data were analyzed by one-way ANOVA by using GraphPad Prism software (version 5.02). The level of significance was set at $p < 0.05$.

3. Results and discussion

3.1 Surface modification, DLS and protein loading analysis

The surface of MCM-41 nanoparticles was modified by APTES, PMMA, PEG and chitosan to determine the interaction with other surfaces and to generate different electrochemical environments (negatively and positively charged) and their subsequent effect on particle size, PDI and zeta potential values. DLS measurements (Table 1) revealed that unmodified MCM-41 nanoparticles were unimodal in distribution and possessed average hydrodynamic diameter in solution between 146 to 321nm but the size increased after surface modification.

After functionalization by amino group (APTES) the surface charge changed from negative to positive with a zeta potential value from -37 to +33mV, while particle size changed from 146 to 175nm. This indicates that, protonated NH_3^+ groups have dominance on the surface of MCM-41 which remains in the protonated state in the neutral deionized water media. After

adding protein to the nanoparticles' suspension, the surface charge properties changed from positive back to negative and zeta potential value from +33 to -45mV and particles size also increased from 175nm to 203nm. This is because OVA has a net negative charge and nanoparticle synthesis was conducted under neutral conditions. OVA EE also increased from 32% for plain MCM-41 to 69% for surface modified MCM-41 APTES and could be due to positive and negative charge interaction between the OVA and APTES respectively. The size distribution of nanoparticles indicates homogenous distribution according to PDI values in Table 1. The rapid decline of charge properties after APTES modification of MCM-41 nanoparticles is due to adsorbing more protein compared with unmodified MCM-41 nanoparticles.

MCM-41 PMMA modified nanoparticles showed, higher size at 211 ± 4nm and PDI of 0.47 ± 0.10 and decreased zeta potential value of 17 ± 2mV after protein loading. In this case neutral charge properties of PMMA co-polymer affected the MCM-41 surface charge (negative to neutral) and colloidal stability (zeta potential) rapidly declined due to the polymer instability in aqueous media. In addition, PDI value indicated that the particle size distribution was multimodal and not homogenous. This suggests that, the electrostatic interaction between co-polymer PMMA and MCM-41 nanoparticles reduced due to the neutral surface charge. The above result could be attributed to the fact that the organic polymer molecule blocked the pore channels of the MCM-41 particles. Interestingly, after OVA encapsulation, the surface charge of particles changed from neutral to negative due to OVA having its own negative charge properties which was dominant in the MCM-41-PMMA formulation but with a very low protein EE at 23%.

Before functionalization, surface charge of the MCM-41 nanoparticles was negative and remained negative after PEG modification with particle size of 236 ± 5nm, PDI of 0.32 ±

0.16 and zeta potential value -33 ± 6mV before protein loading. The phenomenon might be attributed to different chain lengths arising from the significant increase ($p < 0.05$) in particle size after modification, while the PDI value indicated homogenous particle size distribution. Further, after PEG modification, MCM-41 showed an increase in OVA EE from 39% to 67% due to changing surface charge after PEG modification (negative to positive) which had a strong electrostatic interaction with the highly negative encapsulated protein.

After chitosan modification, particles size MCM-41 increased to 321 ± 11nm and zeta potential value changed from -37 ± 3 to 33 ± 4mV, which indicates that chitosan dominates in the modified MCM-41 nanoparticles. MCM-41 particles in water are negatively charged at the studied neutral media, because the hydroxyl groups on their surfaces are deprotonated. Both components (silica and chitosan) within this water pH range displayed intermediate charges and gradually become more positive as chitosan concentration increased due to the protonation of its amine group. In this study, 0.1% chitosan solution was employed for MCM-41 surface modification due to aggregation and formation of large particles at higher chitosan concentrations. After OVA loading, chitosan modified MCM-41 nanoparticles changed the surface properties from neutral to negative charge and zeta potential value and protein EE (74%) also increased and this might be because native OVA is negatively charged. During *in situ* modification of MCM-41 nanoparticles, hydrogen bonds between acetyl groups of the chitosan molecules and hydroxyl groups on the MCM-41 surface have been suggested to provide additional driving force for protein adsorption [19].

3.2 Morphology of MCM-41 modified nanoparticles

SEM image of unmodified MCM-41 blank (Figure 1) nanoparticles and surface modified nanoparticles (Supplementary data, Figure S1A) demonstrate that both showed uniform and spherical shapes. It was also observed that there was no agglomeration of particles after surface

modification. The size of polymer modified MCM-41 nanoparticles was slightly larger than unmodified MCM-41 nanoparticles. In addition, though the particle size from DLS measurement and SEM showed differences, they did not vary considerably as shown by the size distribution histogram (Figure 1B). After OVA encapsulation, nanoparticles showed agglomeration with the unmodified MCM-41 nanoparticles generally showing irregular shapes (figure 1, Image E), which suggests that protein adsorption or encapsulation by nanoparticles could cause aggregation. In comparing between blank and protein loaded nanoparticles using STEM, the images shown in figure 1, image C and image G, depicts homogenous blank nanoparticles which become non-spherical agglomerates after protein encapsulation. In figure S1B (Supplementary data), STEM image of blank nanoparticles showed smooth distinct shapes with clear distances between them, while protein encapsulated nanoparticles (Supplementary data, figure S1B), depict narrow particle size distribution.

3.3 X-Ray Diffraction (XRD) analysis

Investigation of plain MCM-41 nanoparticles, PMMA and chitosan surface modified MCM-41 blank and protein encapsulated nanoparticles showed no sharp peaks suggesting they were amorphous in nature. Both PEG and APTES modified MCM-41 nanoparticles and their blank and OVA encapsulated nanoparticles in figure 2a and figure 2b showed reduction in sharp peaks after formulation of MCM-41 nanoparticles and surface modification compared to the pure starting materials (Figure S2, Supplementary data).

In addition, XRD pattern in figure 2b showed slight shifting of peaks from 26° to 23° 2θ for the PEG modified MCM-41 nanoparticles. PMMA and chitosan modified MCM-41 nanoparticles showed amorphous nature in both blank and OVA encapsulated particles, while the crystalline peaks was observed in PEG modified MCM-41 nanoparticles was in both blank and protein encapsulated formulations. In comparing the diffractograms of pure PEG

(supplementary data) with both blank and OVA encapsulated PEG modified MCM-41 nanoparticles, reduced peak intensities were observed in nanoparticle formulations. This can be attributed to pure OVA and unmodified MCM-41 nanoparticles both of which were amorphous in nature. The XRD results were complemented by DSC analysis data as shown in Figures S3, S4 and S5 (Supplementary data).

3.4 ATR-FTIR

The ATR-FTIR spectra of MCM-41 surface modified nanoparticles are shown in figures 3a and 3b, and that for pure materials (OVA, PEG, CTAB, chitosan) are shown in Figure S6 (Supplementary data). The blank and OVA encapsulated nanoparticles showed absorption peaks arising from asymmetric vibration of Si-O-Si ($1025cm^{-1}$, $1050cm^{-1}$) and asymmetric vibration of Si-OH ($955cm^{-1}$, $910cm^{-1}$) associated with the formation of condensed silica structure [20] [21]. The two bands with weak intensities at 2855 and $2922cm^{-1}$ can be attributed to the stretching vibrations of alkyl chains on the surface from the CTAB coating the MCM-41 nanoparticles as was reported in (Mansfield *et al.*, 2018) [22] A broad and intense peak at $3315cm^{-1}$ is attributed to the stretching vibrations of hydrogen bonds and Si-OH groups covering the surface of the colloidal silica, H-bonding of H_2O and H-bonded OH group. The OVA encapsulated MCM-41 showed various small peaks between 1600 and $1900cm^{-1}$ with the major one peak at $1656cm^{-1}$ being attributed to amide I (a represents a shift to higher wavelength from that of the pure OVA - $1638cm^{-1}$) and a smaller one at $1592cm^{-1}$ due to amide II of OVA. This confirms that the OVA has been encapsulated within the nanoparticles as intended.

Furthermore, peaks appearing at $1470cm^{-1}$ and $1710cm^{-1}$, were attributed to the stretching vibration of a primary carbonyl absorption peak and bending vibration peak of C-H of OVA loaded MCM-41 nanoparticles. Figure 3a and 3b also exhibited a number of characteristic spectral bands, such as; the peaks at $578cm^{-1}$, $690cm^{-1}$ and $789cm^{-1}$ due to the

asymmetric stretching vibration, symmetric stretching vibration and bending vibration of Si-O-Si , while the antisymmetric stretching vibration band around 980cm^{-1} is due to stretching vibration of Si-OH .

APTES modified MCM-41 nanoparticles exhibited CH_2 bending peaks at 1563cm^{-1} while the peaks at 2950 and 3300cm^{-1} corresponding to CH and NH stretching respectively. NH_2 group derived from the APTES and NH stretching indicate the presence of amino groups in the MCM-41 nanoparticles. The PEG modified MCM-41 nanoparticles showed the incorporation of an ester linkage which is proved by the absorption peak at 1472cm^{-1}. MCM-41 PMMA modified nanoparticles sample showed peaks at 172 and 1467cm^{-1} assigned to the carbonyl (C=O) stretching and the CH_2 bending modes, and an absorption peak of Si-O-Si vibration at 1100cm^{-1} indicating (C-O-C) of PMMA overlapping with MCM-41 nanoparticles. The characteristic bands of benzene ring band around 1500cm^{-1} appeared weak in the spectra of MCM-41 PMMA nanoparticles. Chitosan modified MCM-41 nanoparticles showed band shifts from pure materials at 1810cm^{-1} representing NH_2 group deformation vibration. Intensive absorbance at 1110cm^{-1} represents the Si-O stretching vibrations.

3.5 *In vitro* protein release study

The OVA from modified and unmodified MCM-41 nanoparticles was performed in SGF without pepsin (pH = 1.2) and SIF (pH = 6.8) at 37ºC and the results are presented in figures 4a and 4b. Pepsin was not used in OVA encapsulated nanoparticles SGF analysis to avoid technical error caused by interference by pepsin in accurately measuring OVA molecule by Bradford protein assay. However, the stability analysis for the blank nanoparticles was performed in SGF containing pepsin (Figure S7, Supplementary data). The retention of protein activity after passing through the acidic environment of the stomach is a vital functional characteristic for an oral protein delivery carrier. However, to assure absolute stability of OVA

in actual SGF containing pepsin, another protein analysis technique such as LC-MS, which will allow the distinguishing between pepsin in SGF and OVA from the nanoparticles, will be useful in the future.

Non-encapsulated and encapsulated OVA was found in SGF within 30 mins, with the release from PEG and chitosan modified MCM-41 nanoparticles being significantly delayed compared with unmodified and APTES and PMMA modified MCM-41 nanoparticles. In SGF (pH 1.2) 24% of OVA was released from plain MCM-41 within 30 mins and 40% protein within 2 hrs, whilst 25% and 20% of protein was released from MCM-41 PEG and MCM-41 chitosan respectively within 2 hrs. This suggests that most of the encapsulated protein in MCM-41-PEG and MCM-41-chitosan was protected from the gastric environment over a 2 hr period.

PEG modification of MCM-41 resulted in a higher protein release than chitosan due to PEGylating in the dispersion medium which favors protein diffusion [23] suggesting that OVA released from porous nanoparticles depend on the amount of OVA encapsulated into the nanoparticles and free pore volume. Various research papers [24, 25] showed that chitosan is more stable in GIT environment than other natural polymers. The retention time of particles in the stomach is between 1 and 2 hrs. Therefore, since the amount of OVA released at pH 1.2 from PEG modified particles was 16-25% and 14-20% from chitosan modified it is important to optimize the system further in order to provide a minimum contact between gastric environment and protein and thus avoiding any possible protein denaturation. When nanoparticle powder was dispersed in SIF, OVA released from nanoparticles occurred at a slower rate compared with SGF. An initial burst release of protein from modified and unmodified MCM-41 nanoparticles within 1 hr, was followed by sustained release pattern with OVA released very slowly from the nanoparticles. The initial burst release of OVA molecules from MCM-41 nanoparticles could probably be due to the OVA molecules adsorbed on the surface. The reason for the gradual and sustained release of OVA molecules from modified

MCM-41 nanoparticles may be explained as follows: silica nanoparticles after OVA incorporation increased in size which significantly reduced the release rate of OVA, which also applies to low molecular weight compounds as reported by other authors [26]. The MCM-41 APTES, PEG and chitosan modified nanoparticles showed more sustained release pattern compared to unmodified and PMMA modified [27]. These differences may be attributed to a combination of factors, dependent on the silica architecture, including nanoparticles size, pore diameter and charged properties [28]. Meanwhile, the diffusion hindrance from long polymeric chain would prevent the incorporation of OVA molecules into the MCM-41 nanoparticles. APTES, PEG and chitosan modified MCM-41 nanoparticles showed micro pores resembling honeycomb structures which allowed the entry of OVA molecules into the nanoparticles, thereby improving interactions between OVA molecules and the nanocarriers leading to a slower release profile of OVA in SIF.

3.6 Stability analysis of MCM-41-nanoparticles in simulated fluid based on particle size, PDI and zeta potential:

During formulation development of OVA encapsulated nanoparticles, it is very important that chemical and conformational structure of OVA is preserved in order to maintain the biological and pharmacological activity of the entrapped protein. Therefore, stability of the MCM-41 surface modified nanoparticles in two different simulated fluid SGF and SIF was investigated at various time intervals by measuring nanoparticles size, PDI, zeta potential (DLS) and morphology (SEM). The stability of protein loaded MCM-41 nanoparticles evaluated are shown in Figure 5a for SGF and in figure 5b for SIF. Unmodified MCM-41 nanoparticles showed a slight decrease of particle size in SGF after 3 hrs but the nanoparticles were stable in SIF over 4 days as confirmed by SEM images (image not shown).

In SGF, the size of unmodified MCM-41 decreased ($p > 0.05$) from 146nm to 137nm within 3 hrs and showed another steep decrease after 8 hrs and could not be observed by SEM analysis (SEM image not shown). However, the stability of silica nanoparticles in simulated fluids (SGF or SIF) is strongly dependent on pH. At pH values above 7, there is increased deprotonation of silanol groups and hydrolysis of Si-O-Si bonds which is catalyzed by nucleophilic attack of OH ions. Consequently, silica nanoparticles are more stable in SGF pH [29]. However, Valeti and co-workers reported that silica nanoparticles also comprise titratable SiOH groups which can protonate or deprotonate at neutral pH, and further that the particles respond to alkaline pH (>7) resulting in greater negative charges [30].

For APTES modified MCM-41 nanoparticles, the size was decreased ($p > 0.05$) from 175nm to 109nm after 8 hrs, while PDI and zeta potential values also decreased after 4 hrs [25] demonstrating that amino group plays an important role in the erosion of silica nanoparticles. Figure 5a showed that PMMA, PEG and chitosan modified nanoparticles exhibited better stability than APTES and unmodified MCM-41 nanoparticles. After 12 hrs in SGF, polymer modified MCM-41 nanoparticles was observed by SEM (image not shown) and the nanoparticles shape did not indicate any aggregation or erosion. For MCM-41 PMMA nanoparticles, the size was 197nm after 12 hrs and slowly reduced in size after 10 hrs where the size was observed at 118nm. Furthermore, PDI and zeta potential values also decreased (data not shown). The MCM-41 PEG modified nanoparticles showed nanoparticles stability over 12 hrs but some aggregation was observed in SEM images after 8 hrs. After 2 hrs, nanoparticles size was measured at 214nm and after 10 hrs nanoparticles size reduced to 180nm. The MCM-41 chitosan modified MCM-41 nanoparticles showed size of 316nm after 2 hrs and 278 nm over 12 hrs.

According to particles size analysis by DLS and SEM measurements the most stable formulations were MCM-41 PEG and chitosan modified nanoparticles. As was the case for

SIF, PEG and chitosan modified nanoparticles showed the slowest decrease in particle size in SIF confirming them to be the most stable among the four modified silica nanoparticles. At intestinal pH (6.8), unmodified MCM-41 nanoparticles showed, significant reduction ($p < 0.05$) of particle size from 149nm to 60nm in 96 hrs, most likely due to nanoparticles surface molecule undergoing hydrolysis at this pH. Therefore, to avoid this corrosive effect in nanoparticles structure, modification of nanoparticles surface with other functional groups would potentially be an advantage for achieving sustained release of antigen at intestinal pH. In figure 5b, APTES modified MCM-41 nanoparticles showed particle size reduced ($p > 0.05$) from 179nm to 126nm within 12 hrs, which can be explained by possible erosion of loose nanoparticle aggregates. PEG and chitosan modified MCM-41 nanoparticles showed negligible size reduction within 48 hrs and remained stable until 96 hrs.

The results suggest that, the stability of MCM-41 silica nanoparticles depends on their structure as well as the processing conditions. For example, the MCM-41-PEG modified nanoparticles were prepared at higher temperature (80ºC) to form core silica shell nanoparticles resulting in higher levels of polymerization, which showed better stability compared with unmodified MCM-41. It is possible that covalent pegylation on the nanoparticles surface would work as a driving force, maintaining particle dispersion and reducing aggregation tendencies, due to reduced carboxylic groups on the surface [26]. Recently some reports [1] indicated that the presence of pore structures in unmodified silica nanoparticles also influences their stability in simulated fluids. The large surface area is due to high porosity which may lead to more vigorous erosion from the surrounding materials [27]. In addition, the encapsulation of external molecules in silica networks may also trigger disintegration of particles' structure. Therefore, surface modification with amino and polymeric bearing groups could improve their stability, as has been shown in this study.

3.7 Mucin binding analysis

Since the ultimate objective of the surface modified silica nanoparticles was potential delivery to intestinal mucosa to achieve mucosal immune response, their mucoadhesive behavior was investigated by measuring the amount of mucin binding with the nanoparticles by Bradford protein assay. It has been reported [31] that MCM-41 nanoparticles showed low attraction with mucin and therefore required surface modification. It was observed (Table 2) that polymer modified MCM-41 nanoparticles showed good binding capability to mucin compared with the plain MCM-41 nanoparticles, with the unmodified MCM-41 nanoparticles showing mucin binding of 19% whilst PEG and chitosan modified nanoparticles showed 57 and 49% binding respectively. PEG and chitosan act as mucoadhesive polymers due to enhanced electrostatic interaction between negatively charged sialic acid residue of mucin and positively charged PEG and chitosan on modified MCM-41 nanoparticle surfaces. However, according to Table 1, the modified MCM-41-PEG nanoparticles, which showed the highest mucin binding, were negatively charged with zeta potential value of -33mV. This will suggest that other mechanisms and factors beside the electrostatic interaction (possibly hydrogen bonding and van de Waals forces might be contributing to the mucin binding; however, this will require further investigation.

The mucoadhesive properties of chitosan and PEG are based on the hydrogen bonding between polyethylene oxide group of PEG and amino groups from chitosan. This interaction is very important to understand the cell interaction of nanoparticles leading to uptake and is an important requirement of mucosal delivery of therapeutics. APTES and PMMA modified nanoparticles showed lower mucin binding values of 26% and 41 % respectively compared with PEG and chitosan modified MCM-41 nanoparticles, due to the natural mucoadhesive properties of PEG and chitosan.

3.8 Circular dichroism analysis of *in vitro* released OVA

Circular dichroism (CD) is an excellent and sensitive method for rapidly evaluating the secondary structure, folding and binding properties of proteins and various research papers [32, 33, 34] have reported the detection of structural changes of proteins after interacting with nanoparticles. The CD spectra of OVA released from the various formulations are shown in in figure 6. In the case of MCM-41 PMMA, the OVA interaction with MCM-41 nanoparticles caused a clear change in the CD spectrum compared with the native protein. An analysis carried out using a set of reference CD spectra for α-helix, β-sheet, and irregular structures indicates that in the MCM-41 nanoparticles system the α-helical content of protein molecule were limited and probably resulting in an increase in the irregular structures. In the case of MCM-41 APTES, the intensity of CD spectrum decreased significantly compared to the pure OVA, while retaining the original shape, indicating that the protein precipitates upon interaction with MCM-41 APTES nanoparticles. This effect was also seen during DLS analysis in Table 1 which showed the formation in solution of some aggregates and large sized particles. The CD spectrum of OVA released from PMMA modified MCM-41 nanoparticles showed significant difference compared with pure OVA sample. The CD spectrum of OVA consists of α-helix signals including π-π at 208 and n-π at 220nm wavelength and its denaturation resulted in an attenuation of these CD signals. The CD spectra of OVA from PEG and chitosan modified sample, showed no significant difference from spectrum of pure OVA sample, and suggested that the protein underwent no significant denaturation on encapsulation and release from both modified MCM-41 nanoparticles. The porosity of these particles could play significant role in ensuring the maintenance of protein structure. At pH 6.8 OVA molecules would have significant negative charge and this charge build up within the constructed environment in the pores of the PEG and chitosan modified MCM-41 surface would have resulted in a greater

degree of stability of the protein structure than the other nanoparticles with smaller pore sizes, therefore predominantly possessed surface adsorbed protein.

3.9 SDS–PAGE analysis:

Evidence for the presence of OVA during *in vitro* release from the nanoparticles was further confirmed using SDS-PAGE (Figure 7). SDS-PAGE is an excellent technique for separating macromolecules based on their weight as well as under the influence of an electric field and is therefore termed electrophoresis [35]. Bands were observed at 44kDa and no other bands were observed in comparison with pure OVA band (A) (figure 7), suggesting that the particles did not cleave the protein which indicates that the primary structure of the protein was not affected by the harsh nanoparticles formulation processing conditions. Uddin and Gill reported that OVA solution showed the presence of additional protein bands attributed to small quantities of ovotransferrin (76kDa) and lysozyme (14.4kDa) impurities, which are the two abundant egg white proteins [36] and which they referred to as residual proteins [37]

3.10 Brunauer-Emmett-Teller (BET) analysis:

Nitrogen-adsorption and desorption techniques were used to analyze the surface area, pore volume and pore size distribution of the formulated MCM-41 nanoparticles. Figure 8 exhibited typical type II isotherm as well as ordered porous structure, as judged by the hysteresis loops [38]. The BET surface area (S_{BET}), pore volume (V_p) and pore diameter distribution are summarized in Table 3. MCM-41 blank nanoparticles in comparison with APTES and PMMA modified MCM-41 nanoparticles showed reduction in pore size from 5nm to 2.8 and 2.3nm respectively, after the modification which might be attributed to the blockage of pores during drying process. However, PEG and chitosan modified MCM-41 nanoparticles displayed high surface areas of $621 m^2 g^{-1}$ and $641 m^2 g^{-1}$, pore sizes of 3.2 and 3.5, as well as large pore volume

0.80 and 0.77 cm^3/g respectively. This is because the surface group introduced increased the mass of the sample and formed a part of the pore volume. The unchanged hysteresis loops and pore size confirmed that pores were not blocked during MCM-41 surface modification. In comparing between MCM-41 and functional modification of MCM-41 nanoparticles, it can be inferred that the distribution of the micropores shift or tails toward somewhat larger pore sizes as the synthesis temperature is increased. However, the pore diameter achieved for MCM-41 PEG and chitosan modified nanoparticles was comparably higher than that of other research papers [39, 40] and this suggested that these surface modified MCM-41 nanoparticles would be suitable for protein encapsulation.

4 Conclusions

The main objective of this study was to develop strong core shell and porous MCM-41 nanoparticles with surface modification to achieve maximum protein encapsulation and also be able to protect the protein from the harsh gastrointestinal environment to allow delivery to the target site within intestinal Peyer's patches. Surface modified MCM-41 nanoparticles using polymer (PMMA, PEG, chitosan) and amine (APTES) changed their physicochemical properties, influencing the particle size, PDI, zeta potential as well protein loading efficiency and *in vitro* protein release profiles. The APTES, PEG and chitosan modified MCM-41 nanoparticles released OVA in a controlled manner whilst unmodified MCM-41 nanoparticles showed faster release rate. Testing in the presence of simulated fluid (SGF and SIF) suggest that PEG and chitosan modified MCM-41 nanoparticles exhibited excellent stability, as well as high protein encapsulation profile. However, a further optimization of the release profile is required to decrease the protein release in the GIT environment as well as investigating the immunogenicity using an animal in vivo model to confirm the ability of the nanoparticles to deliver vaccines successfully using the oral route. Finally it can be concluded that, PEG and

chitosan modified MCM-41 nanoparticles achieved significant increase of protein encapsulation efficiency in microporous protein host, provided protection of the encapsulated protein without any structural modification, produced spherical particles with appropriate porosity via an easy synthesis process, excellent mucin binding, and possessed high surface area. They therefore show great potential for oral protein-based vaccine delivery.

Figure Legends

Figure 1 A) Representative SEM images of blank surface modified MCM-41 nanoparticle image B) Histogram showing particle size distribution of image A by ImageJ software. C) STEM image of typical blank MCM-41 nanoparticles. D) Histogram showing particle size distribution of image C by ImageJ software. E) Representative SEM image of OVA encapsulated surface modified MCM-41 nanoparticles. F) Histogram showing particle size distribution of image E by ImageJ software. G) STEM image of typical OVA encapsulated MCM-41 nanoparticles. H) Histogram showing particle size distribution of image G by ImageJ software.

Figure 2 XRD diffractograms of (a) MCM-41 blank nanoparticles and (b) MCM-41 surface modified OVA encapsulated nanoparticles.

Figure 3 ATR-FTIR spectra of (a) blank MCM-41 nanoparticles and (b) OVA encapsulated MCM-41 nanoparticles.

Figure 4 *In vitro* protein release profiles (n = 3) of OVA in (a) in SGF (pH 1.2) and (b) in SIF (pH 6.8).

Figure 5 MCM-41 nanoparticles stability studies (n = 3) in (a) SGF (pH 1.2) and (b) SIF (pH 6.8).

Figure 6 CD spectra of OVA released from various nanoparticle formulations

Figure 7 SDS-PAGE analysis of OVA protein in (A) pure native OVA, (B) MCM-41-PEG (C) MCM-41-Chitosan (D) MCM-41-PMMA (E) MCM-41-APTES nanoparticles.

Figure 8 BET surface area measurement of MCM-41 blank nanoparticles.

Declarations of interest: None

References:

[1] Mody KT, Popat A, Mahony D, Cavallaro AS, Yu C, Mitter N. Mesoporous silica nanoparticles as antigen carriers and adjuvants for vaccine delivery. *Nanoscale*. pp 5167-5179, 5(12), 2013.

[2] Bale SS, Kwon SJ, Shah DA, Banerjee A, Dordick JS, Kane RS. Nanoparticle-mediated cytoplasmic delivery of proteins to target cellular machinery. *ACS Nano*. pp1493-1500, 4(3), 2010.

[3] Deng Y, Mathaes R, Winter G, Engert J. Encapsulation of antigen-loaded silica nanoparticles into microparticles for intradermal powder injection. *Eur. J. Pharm. Sci.* pp 154-166, 15(63), 2014.

[4] Xia T, Kovochich M, Liong M, Meng H, Kabehie S, George S, Zink JI, Nel AE. Polyethyleneimine coating enhances the cellular uptake of mesoporous silica nanoparticles and allows safe delivery of siRNA and DNA constructs. *ACS Nano*. pp3273-3286, 3(10), 2009.

[5] Wang T, Jiang H, Zhao Q, Wang S, Zou M, Cheng G. Enhanced mucosal and systemic immune responses obtained by porous silica nanoparticles used as an oral vaccine

adjuvant: Effect of silica architecture on immunological properties. *Int. J. Pharm.* pp351-358, 436(1-2), 2012.

[6] Kim SS, Karkamkar A, Pinnavaia TJ, Kruk M, and Jaroniec M. Synthesis and characterization of ordered, very large pore MSU-H silicas assembled from water-soluble silicates. *J. Phys. Chem. B*, pp 7663-7670, 105(32),2001.

[7] Fan T, Chen C, Guo H, Xu J, Zhang J, Zhu X, Yang Y, Zhou Z, Li L, Huang Y. Design and evaluation of solid lipid nanoparticles modified with peptide ligand for oral delivery of protein drugs. *Eur. J. Pharm. Biopharm.*, pp 518-28, 88(2), 2014.

[8] Kneuer C, Sameti M, Haltner EG, Schiestel T, Schirra H, Schmidt H, Lehr CM. Silica nanoparticles modified with aminosilanes as carriers for plasmid DNA. *Int. J. Pharm.* pp 257-261,196(2), 2000.

[9] Colilla M, Baeza A, and Vallet-Regí M. 'Mesoporous Silica Nanoparticles for Drug Delivery and Controlled Release Applications', in *The Sol-Gel Handbook*, pp 1309-1344, Chapter 42, 2015.

[10] Hao N, Tang F, and Li L. MCM-41 mesoporous silica sheet with ordered perpendicular nanochannels for protein delivery and the assembly of Ag nanoparticles in catalytic applications. *Microporous Mesoporous Mater.* pp 223-227, 218(1), 2015.

[11] Li Z, Barnes JC, Bosoy A, Stoddart JF, Zink JI. Mesoporous silica nanoparticles in biomedical applications', *Chem. Soc. Rev*. pp 2590-2605, 41(7), 2012.

[12] Du X, Shi B, Liang J, Bi J, Dai S, Qiao SZ. Qiao. Developing functionalized dendrimer-like silica nanoparticles with hierarchical pores as advanced delivery nanocarriers. *Adv. Mater.* pp 5981-5985, 25(41), 2013.

[13] Matos JR, Mercuri LP,Kruk M, and Jaroniec M. Toward the synthesis of extra-large-pore MCM-41 analogues. *Chem. Mater.* pp 1726-1731, 13(5), 2001.

[14] Lazzari S, Moscatelli D, Codari F, Salmona M, Morbidelli M, Diomede L. Colloidal

stability of polymeric nanoparticles in biological fluids, *J. Nanopart. Res.* pp 1-10, 14(920), 2012.

[15] Cheung RC, Ng TB, Wong JH, Chan WY. Chitosan: An update on potential biomedical and pharmaceutical applications. *Marine Drugs*. pp 5156-5186, 13(8), 2015.

[16] Ahmed TA, Aljaeid BM. Preparation, characterization, and potential application of chitosan, chitosan derivatives, and chitosan metal nanoparticles in pharmaceutical drug delivery. *Drug Design Dev Ther*. pp 483-507, 28(10), 2016.

[17] Bagwe RP, Hilliard LR, and Tan W. Surface modification of silica nanoparticles to reduce aggregation and non-specific binding. *Langmuir*, PP 4357–4362, 22(9), 2006.

[18] Théry C, Amigorena S, Raposo G, & Clayton A. Isolation and Characterization of Exosomes from Cell Culture Supernatants and Biological Fluids. *Curr. Protoc.Cell Biol.* 30(1), 3.22.1–3.22.29, 2006.

[19] Luo GF, Chen WH, Liu Y, Lei Q, Zhuo RX, Zhang XZ. 'Multifunctional enveloped mesoporous silica nanoparticles for subcellular co-delivery of drug and therapeutic peptide. *Sci. Rep.* pp 1-10, 4(6064), 2014.

[20] Mishra A, Melo JS, Agrawal A, Kashyap Y, Sen D. Preparation and application of silica nanoparticles-Ocimum basilicum seeds bio-hybrid for the efficient immobilization of invertase enzyme. *Coll. Surf. B: Biointerf.* 1-32, 188:110796, 2020

[21] Ahmadi E, Dehghannejad N, Hashemikia S, Ghasemnejad M, Tabebordbar H. Synthesis and surface modification of mesoporous silica nanoparticles and its application as carriers for sustained drug delivery. *Drug Deliv.* 164–172, 21(3), 2014

[22] Mansfield EDH, Pandya Y, Mun EA, Rogers SE, Ionita AI, Danino D, Williams AC and Khutoryanskiy VV. Structure and characterization of hydroxyethylcellulose–silica nanoparticles. *RSC Adv*. 6471–6478, 8, 2018.

[23] Li L, Liu T, Fu C, Tan L, Meng X, Liu H. Biodistribution, excretion, and toxicity of mesoporous silica nanoparticles after oral administration depend on their shape. *Nanomedicine Nanotechnology, Biol. Med.* pp 1915-1924, 11(8), 2015.

[24] Chapa-González C, Piñón-Urbina AL, García-Casillas PE. Synthesis of Controlled-Size Silica Nanoparticles from Sodium Metasilicate and the Effect of the Addition of PEG in the Size Distribution. *Mater*. pp 1-7, 11(4), 2018

[25] Yagüe C, Moros M, Grazú V, Arruebo M, and Santamaría J. Synthesis and stealthing study of bare and PEGylated silica micro- and nanoparticles as potential drug-delivery vectors. *Chem. Eng. J.* pp 45-53 , 137(1), 2008.

[26] Mody KT, Mahony D, Cavallaro AS, Stahr F, Qiao SZ, Mahony TJ, Mitter N. Freeze-drying of ovalbumin loaded mesoporous silica nanoparticle vaccine formulation increases antigen stability under ambient conditions. *Int. J. Pharm.* pp 325-32, 465(1-2), 2014.

[27] Cheng SH, Liao WN, Chen LM and Lee CH. pH-controllable release using functionalized mesoporous silica nanoparticles as an oral drug delivery system. *J. Mater. Chem*, PP 7130-7137, 21, 2011

[28] Tang L, Cheng J. Nonporous silica nanoparticles for nanomedicine application. *Nano Today*, pp 290-312, 8(3), 2013.

[29] Braun K, Pochert A, Beck M, Fiedler R, Gruber J, Linden M. Dissolution kinetics of mesoporous silica nanoparticles in different simulated body fluids. *J Sol-Gel Sci Technol*, pp 1-9, 79(2), 2016

[30] Valetti S, Feiler A,Trulsson M. Bare and effective charge of mesoporous silica particles. *Langmuir*, pp 7343-7351, 33(29), 2017

[31] Andreani T, Miziara L, Lorenzón EN, de Souza AL, Kiill CP, Fangueiro JF, Garcia ML, Gremião PD, Silva AM, Souto EB. Effect of mucoadhesive polymers on the *in*

vitro performance of insulin-loaded silica nanoparticles: Interactions with mucin and biomembrane models. *Eur. J. Pharm. Biopharm.*, pp 118-126 , 93, 2015.

[32] Greenfield NJ, Using circular dichroism spectra to estimate protein secondary structure', *Nat. Protoc.*, pp 2876-2890, 1(6), 2007.

[33] Iranfar H, Rajabi O, Salari R, Chamani J. Probing the interaction of human serum albumin with ciprofloxacin in the presence of silver nanoparticles of three sizes: Multispectroscopic and ζ potential investigation. *J. Phys. Chem. B*, pp 1951-1964, 116(6), 2012.

[34] Satzer P, Svec F, Sekot G, Jungbauer A. Protein adsorption onto nanoparticles induces conformational changes: Particle size dependency, kinetics, and mechanisms. *Eng. Life Sci.*,pp 238-246, 16(3), 2016.

[35] Smithies O. How it all began: A personal history of gel electrophoresis. in *Methods in Mol Biol.* pp 1-21, 1855, Chapter 1, 2019.

[36] Uddin MJ. Gill HS. Ragweed pollen as an oral vaccine delivery system: Mechanistic insights. *J. Contr. Rel*. pp.416-426, 268, 2017.

[37] Uddin MJ, Gill HS. From allergen to oral vaccine carrier: A new face of ragweed pollen. *Int. J. Pharm*. pp 286-294, 545, (1–2), 2018.

[38] Manzano M, Aina V, Areán CO, Balas F, Cauda V, Colilla M, Delgado MR, Regí MV. Studies on MCM-41 mesoporous silica for drug delivery: Effect of particle morphology and amine functionalization. *Chem. Eng. J.*, pp 30-37, 137 (1), 2008.

[39] Yildirim A, Ozgur E, Bayindir M, E. Impact of mesoporous silica nanoparticle surface functionality on hemolytic activity, thrombogenicity and non-specific protein adsorption. *J. Mater. Chem. B*, 1909-1920, 14, 2013

[40] Wiecinski PN, Metz KM, Mangham AN, Jacobson KH, Hamers RJ, Pedersen JA. Gastrointestinal biodurability of engineered nanoparticles: Development of an in vitro

assay. *Nanotoxicol*. pp 202-214, 3(3), 2009.

Table 1: Size, PDI and zeta potential of MCM-41 -surface modified blank and OVA encapsulated nanoparticles measured using DLS.

Formulation	Blank size (nm ± SD)	Blank PDI (± SD)	Blank Zeta potential (mV ± SD)	OVA loaded size (nm ± SD)	OVA loaded PDI (± SD)	OVA loaded Zeta potential (mV ± SD)	OVA encapsulation efficiency (EE) % (± SD)	OVA loading capacity (LC) % (± SD)
MCM-41	146 ± 5	0.21 ± 0.01	-37 ± 3	155 ± 7	0.24 ± 0.02	-39 ± 4	32 ± 2	28 ± 3
MCM-41-APTES	175 ± 6	0.29 ± 0.04	+33 ± 5	203 ± 10	0.22 ± 0.01	-45 ± 9	69 ± 1	58 ± 1
MCM-41-PMMA	211 ± 4	0.47 ± 0.10	+17 ± 2	256 ± 8	0.32 ± 0.01	-36 ± 3	22 ± 4	19 ± 2
MCM-41-PEG	236 ± 5	0.25 ± 0.16	-33 ± 6	287 ± 5	0.46 ± 0.03	-39 ± 2	67 ± 5	53 ± 2
MCM-41-chitosan	321 ± 11	0.37 ± 0.09	33 ± 4	416 ± 12	0.52 ± 0.02	-31 ± 5	73 ± 3	64 ± 1

Table 2: In-vitro mucin binding analysis of MCM-41 nanoparticles.

Formulation	Mucin binding (%)
MCM-41	19 ± 3%
MCM-41-APTES	26 ± 5%
MCM-41-PEG	59 ± 4%
MCM-41-PMMA	41 ± 4%
MCM-41-Chitosan	49 ± 2%

Table 3: BET pore size, pore volume and surface area measurement of blank nanoparticles.

Formulation name	Pore size (nm)	Surface area for nanoparticle (m^2g^{-1})	Pore volume (cm^3/g)
MCM-41	5.0	776	0.86
MCM-41-APTES	2.8	655	0.74
MCM-41-PMMA	2.3	535	0.66
MCM-41-PEG	3.2	621	0.80
MCM-41Chitosan	3.5	641	0.77

15

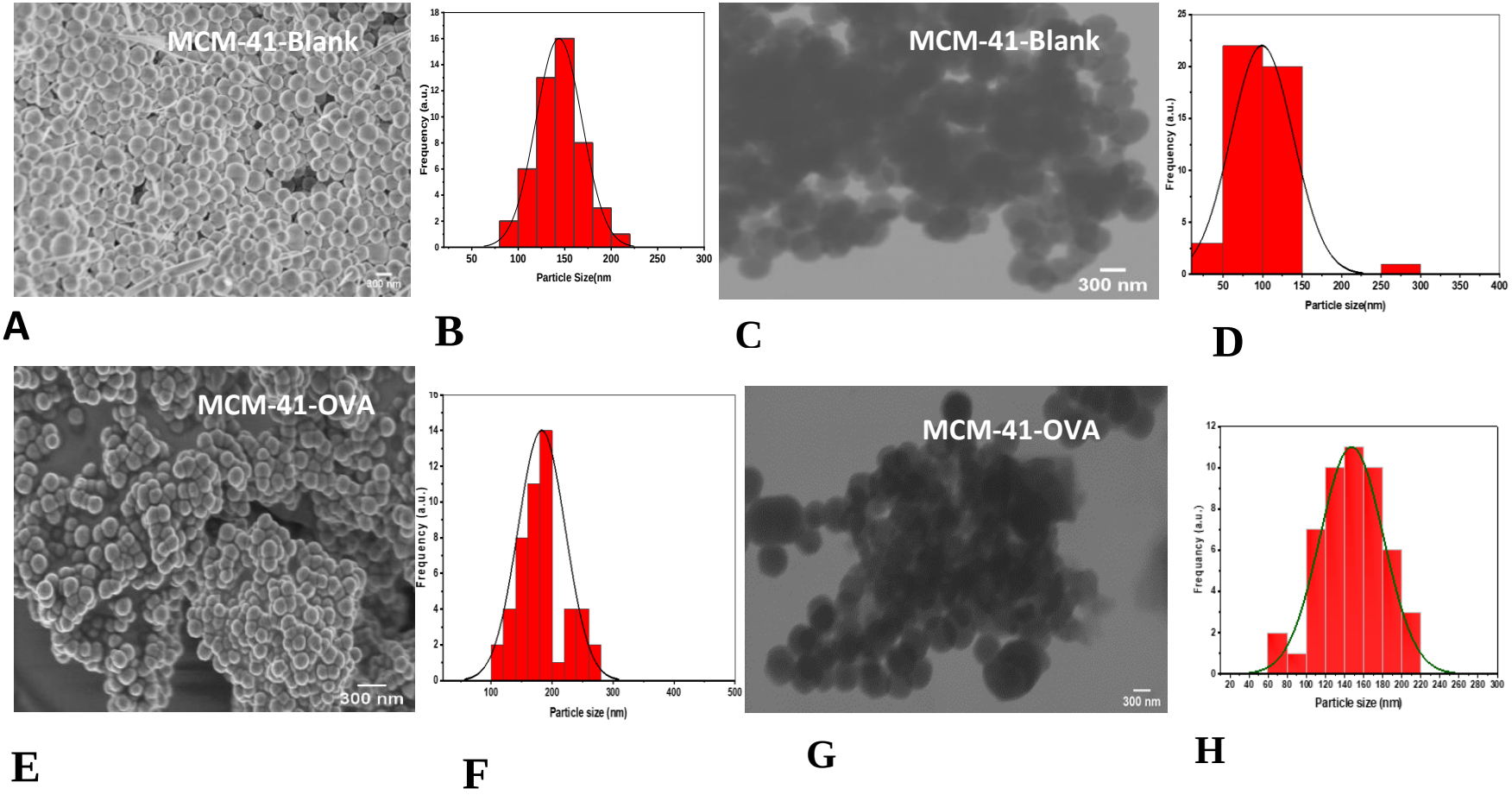

16

17 Figure

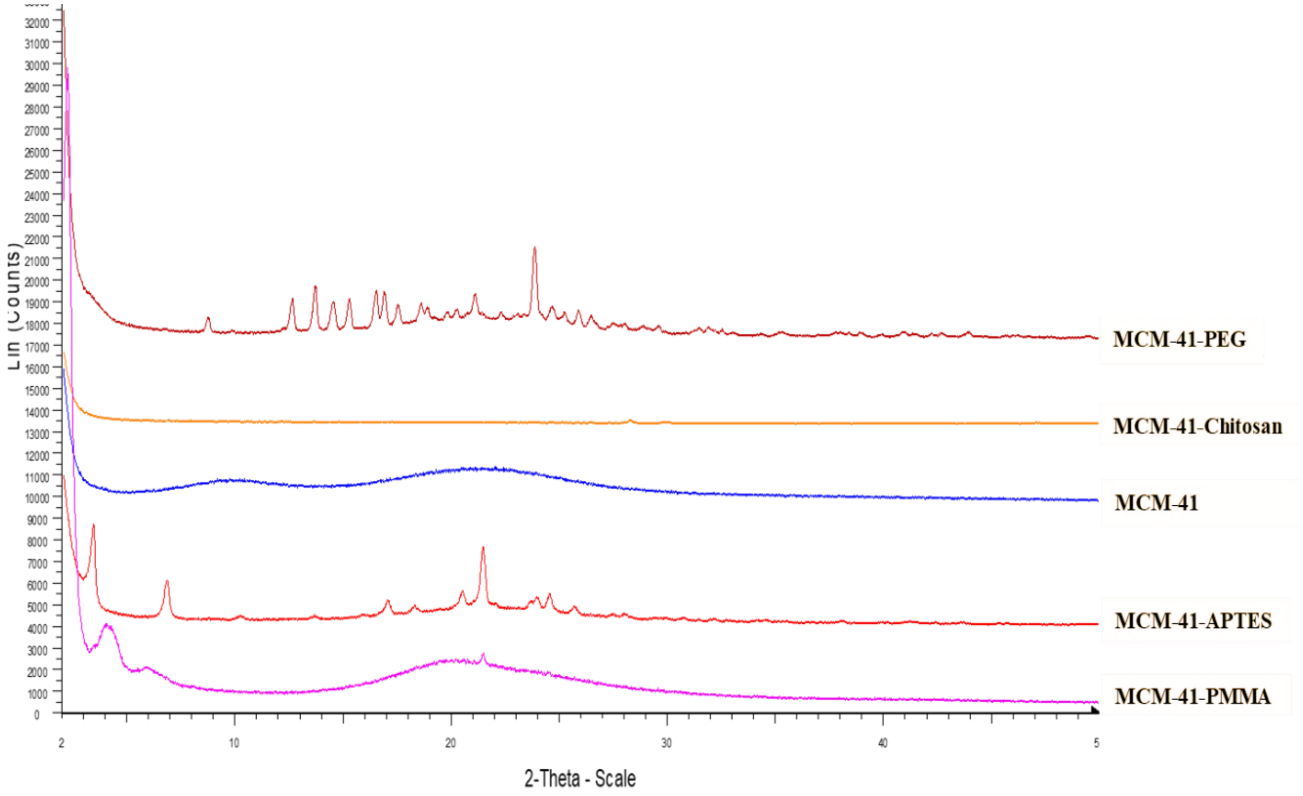
Lin (Counts)
2-Theta - Scale
MCM-41-PEG
MCM-41-Chitosan
MCM-41
MCM-41-APTES
MCM-41-PMMA

(a)

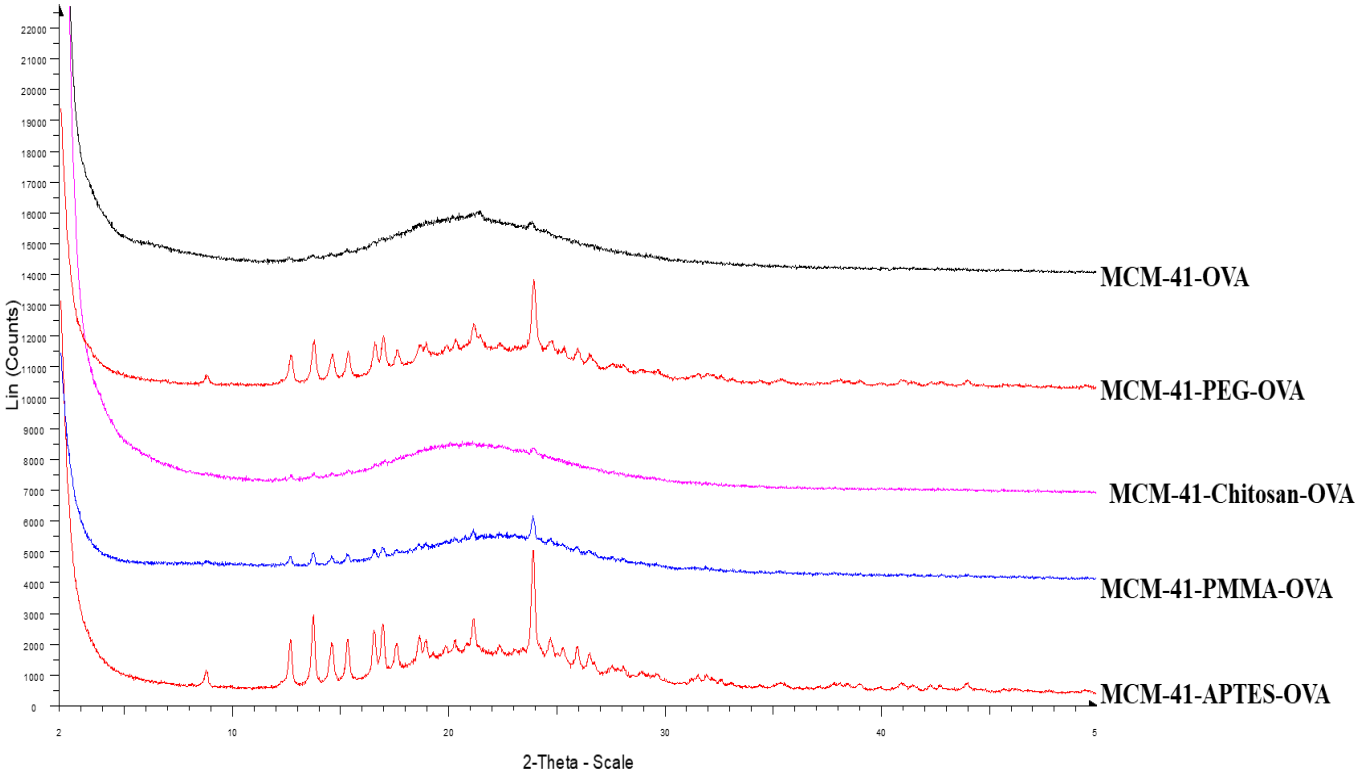
Lin (Counts)
2-Theta - Scale
MCM-41-OVA
MCM-41-PEG-OVA
MCM-41-Chitosan-OVA
MCM-41-PMMA-OVA
MCM-41-APTES-OVA

(b)

Figure 2

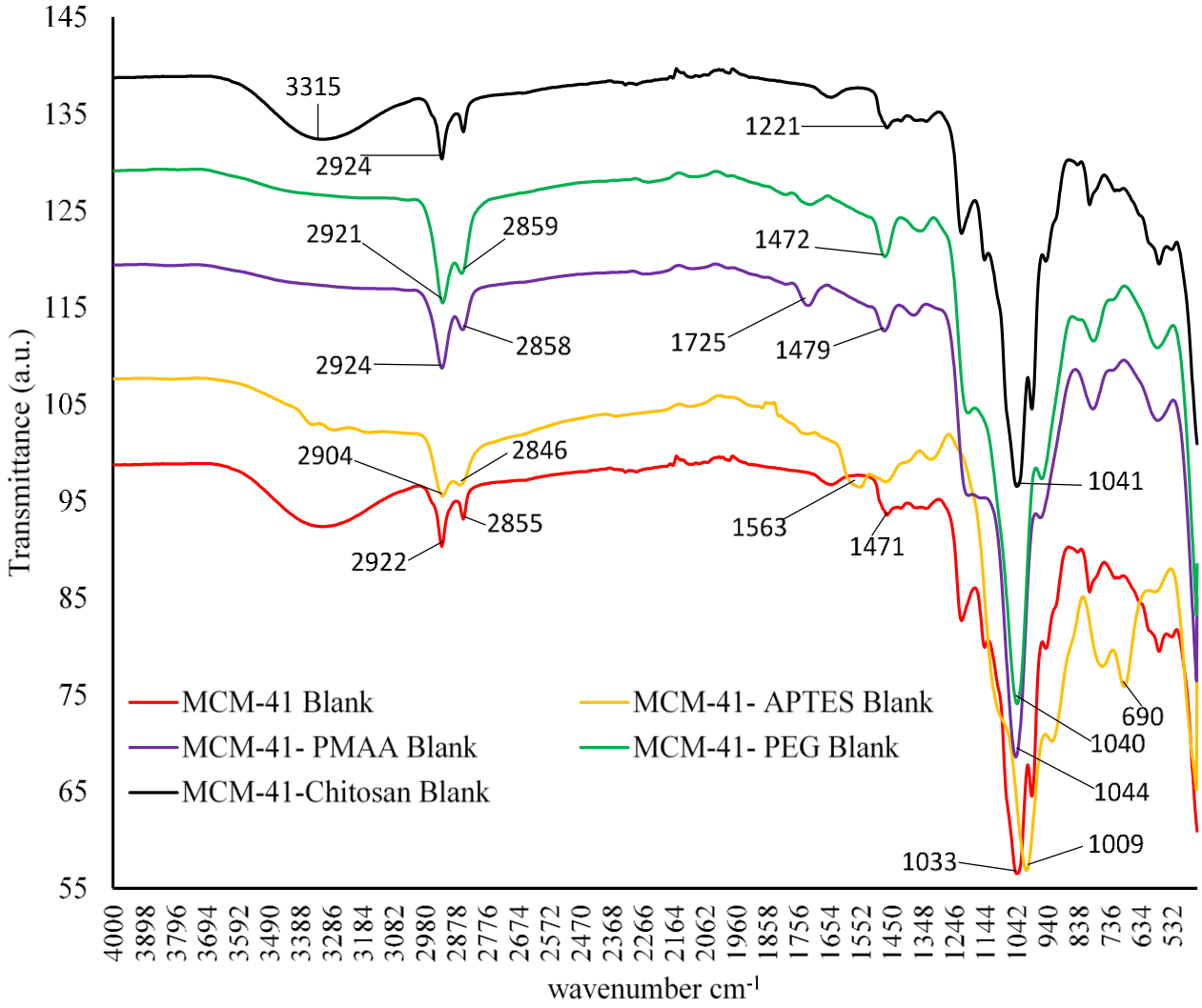
Transmittance (a.u.)
wavenumber cm-1
MCM-41 Blank
MCM-41- APTES Blank
MCM-41- PMAA Blank
MCM-41- PEG Blank
MCM-41-Chitosan Blank
3315
2924
1221
2921
2859
1472
2924
2858
1725
1479
2904
2846
1041
2855
1563
2922
1471
690
1040
1044
1033
1009

23

24 (a)

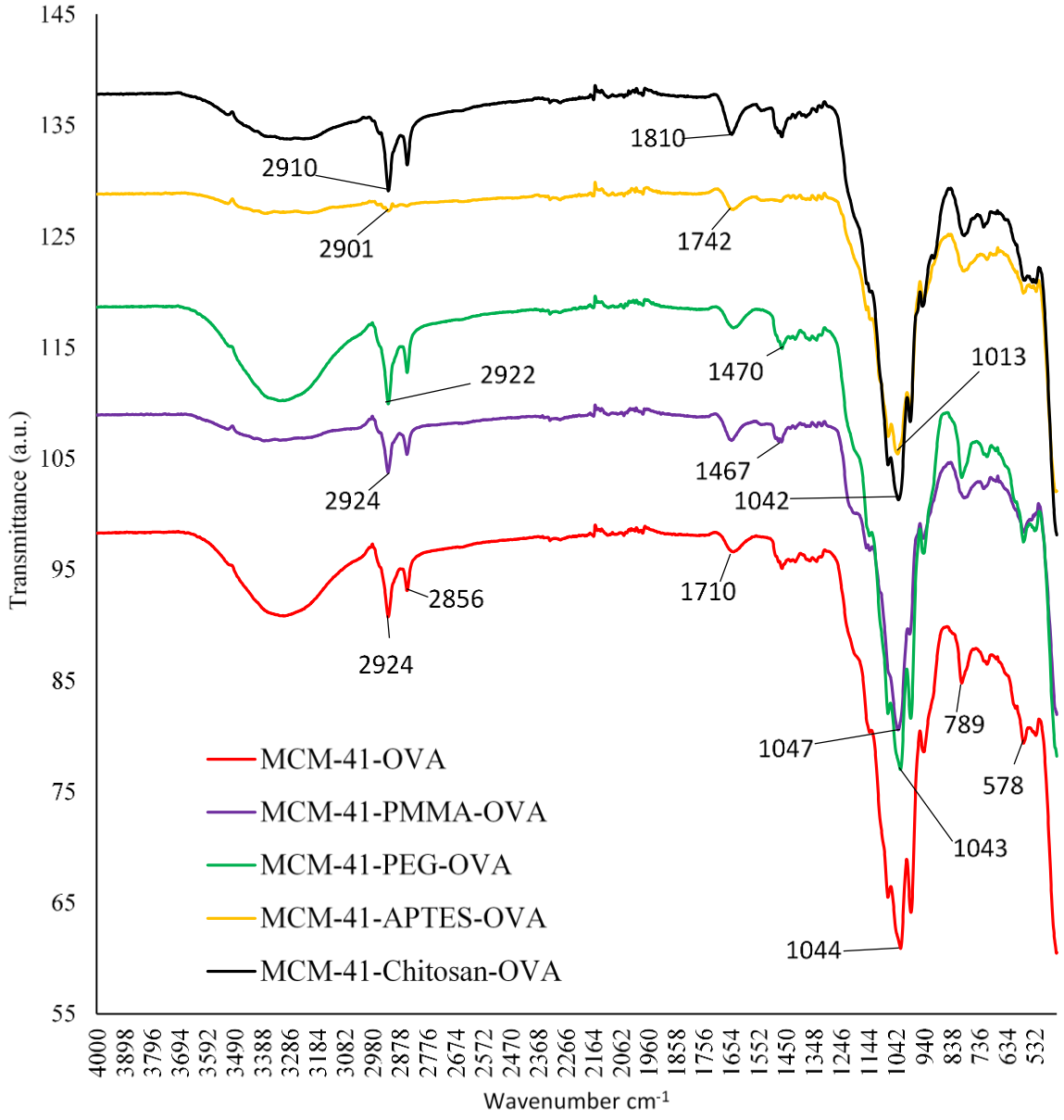

25

26 (b)

27 Figure 3

28

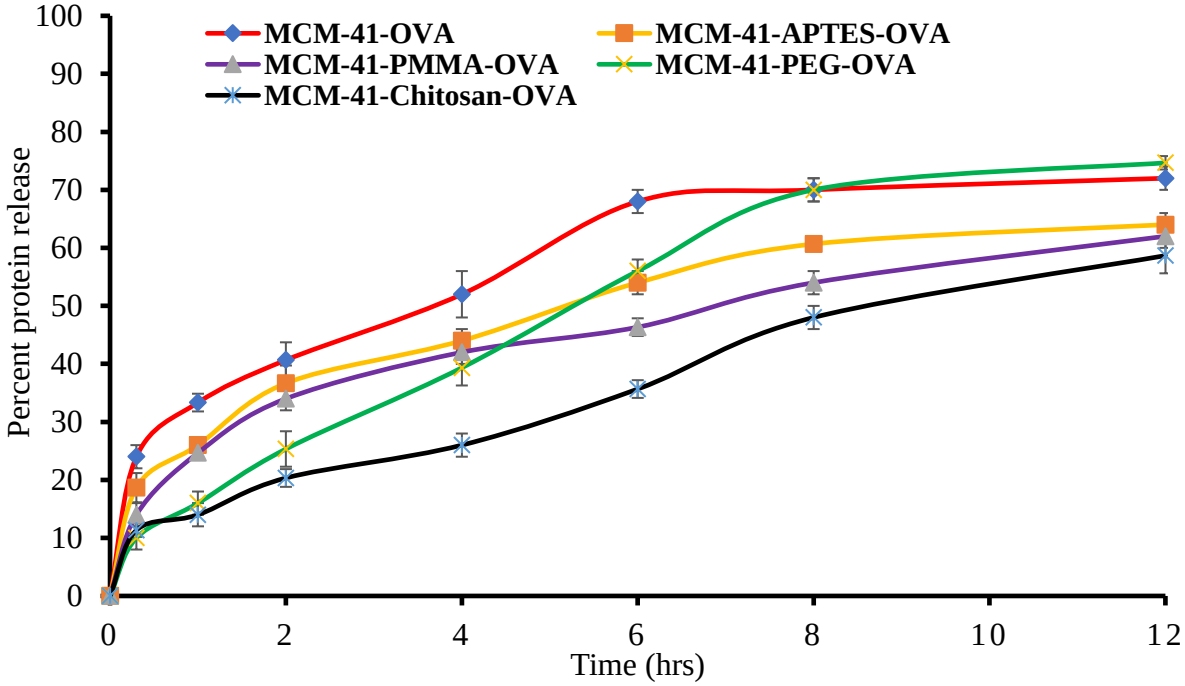
MCM-41-OVA
MCM-41-APTES-OVA
MCM-41-PMMA-OVA
MCM-41-PEG-OVA
MCM-41-Chitosan-OVA
Percent protein release
Time (hrs)
0
10
20
30
40
50
60
70
80
90
100
0
2
4
6
8
10
12

(a)

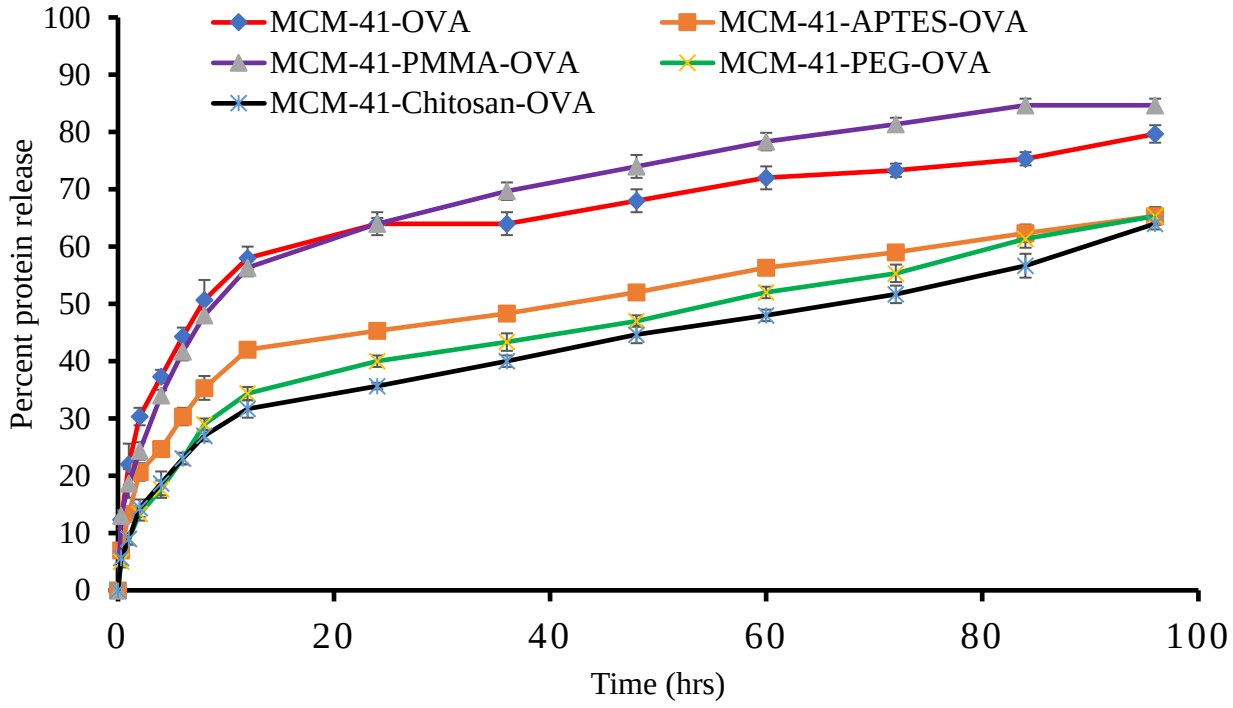
MCM-41-OVA
MCM-41-APTES-OVA
MCM-41-PMMA-OVA
MCM-41-PEG-OVA
MCM-41-Chitosan-OVA
Percent protein release
Time (hrs)
0
10
20
30
40
50
60
70
80
90
100
0
20
40
60
80
100

(b)

Figure 4

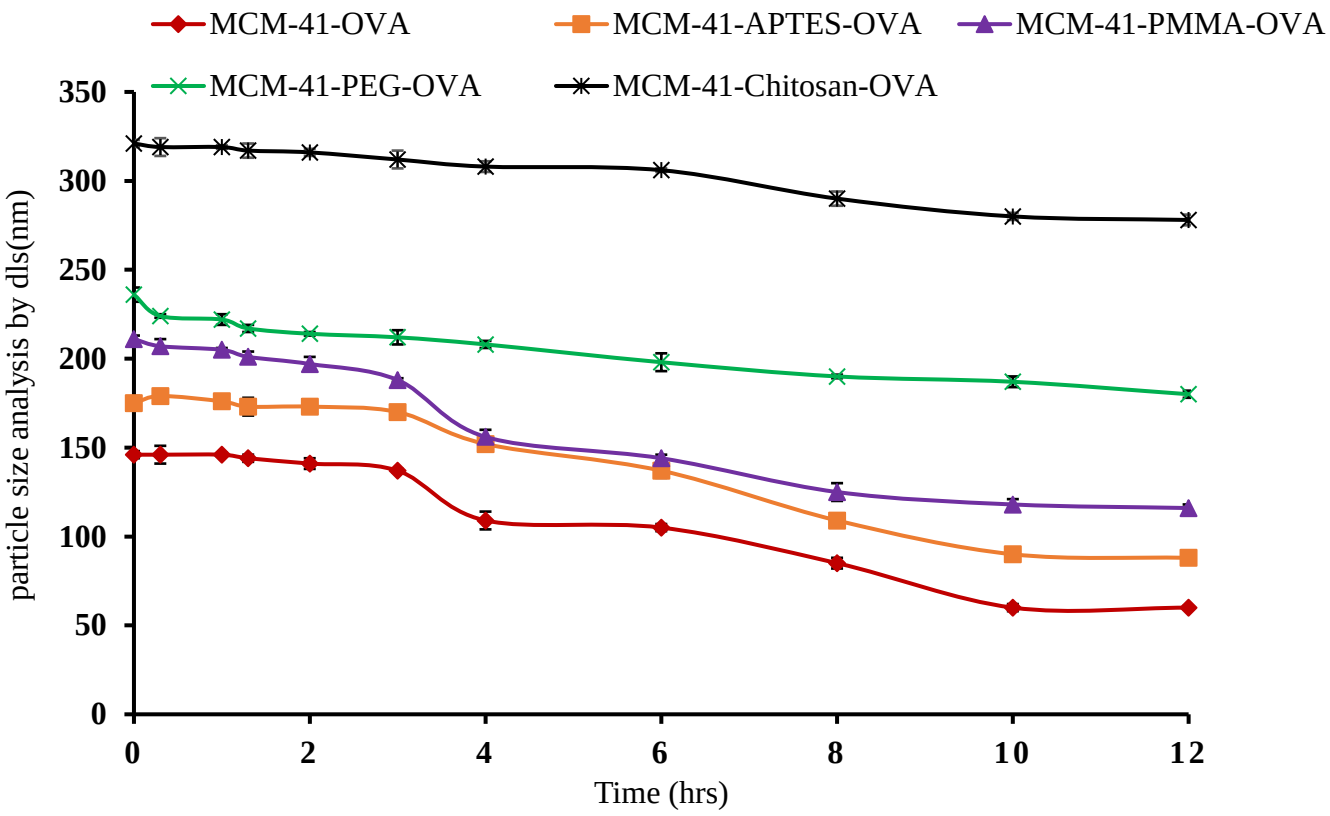
MCM-41-OVA
MCM-41-APTES-OVA
MCM-41-PMMA-OVA
MCM-41-PEG-OVA
MCM-41-Chitosan-OVA
particle size analysis by dls(nm)
350
300
250
200
150
100
50
0
0
2
4
6
8
10
12
Time (hrs)

(a)

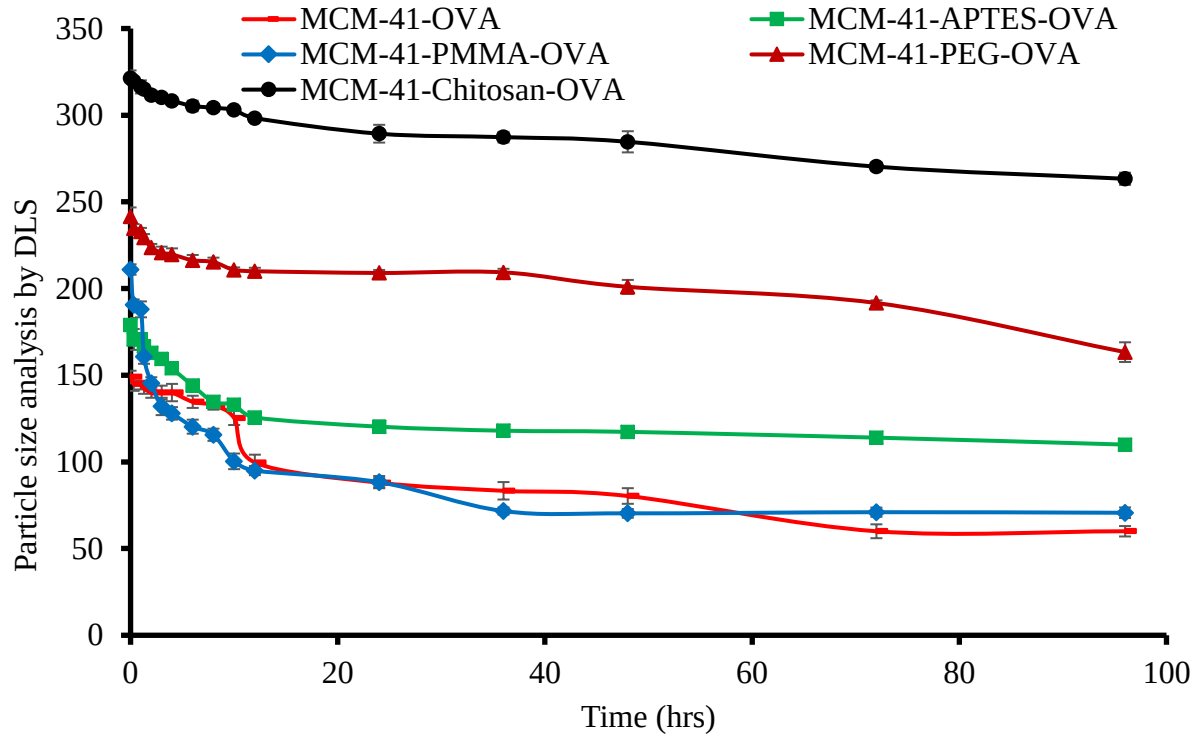
MCM-41-OVA
MCM-41-APTES-OVA
MCM-41-PMMA-OVA
MCM-41-PEG-OVA
MCM-41-Chitosan-OVA
Particle size analysis by DLS
350
300
250
200
150
100
50
0
0
20
40
60
80
100
Time (hrs)

(b)

Figure 5

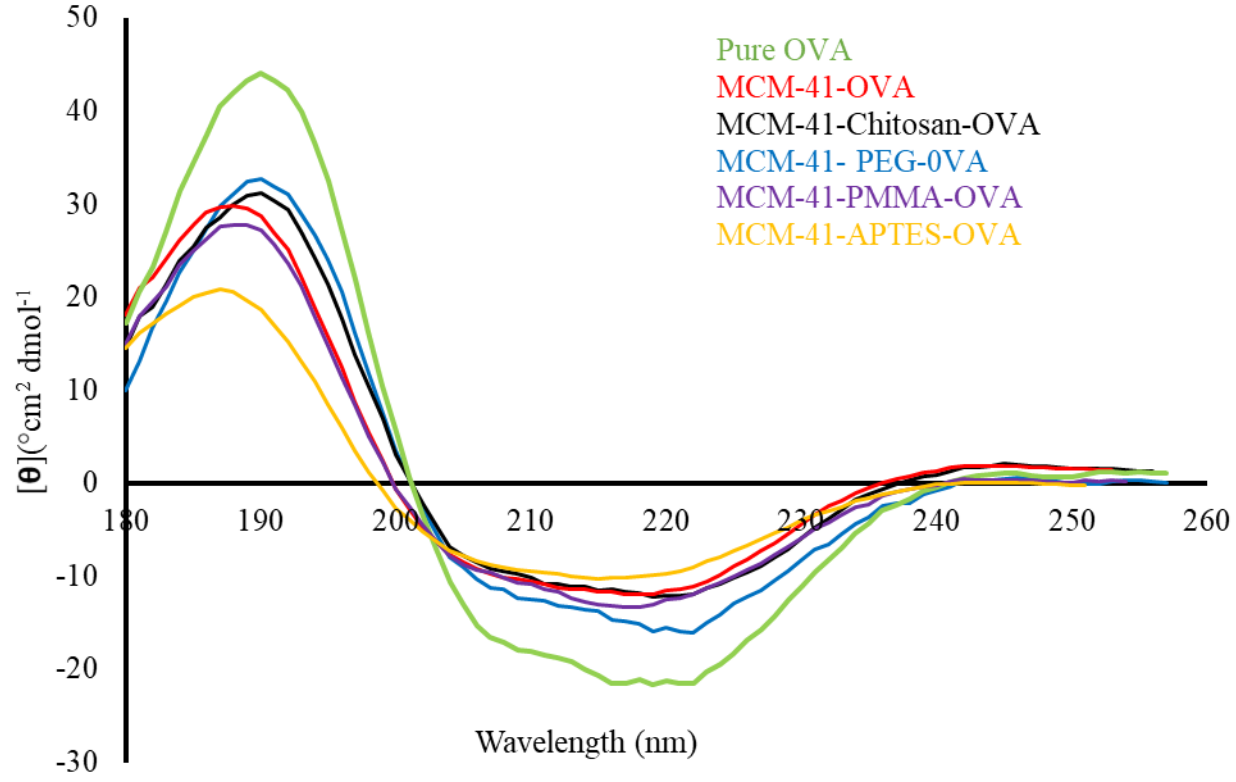
Pure OVA
MCM-41-OVA
MCM-41-Chitosan-OVA
MCM-41- PEG-0VA
MCM-41-PMMA-OVA
MCM-41-APTES-OVA
[θ](°cm² dmol⁻¹
Wavelength (nm)
50
40
30
20
10
0
-10
-20
-30
180
190
200
210
220
230
240
250
260

Figure 6

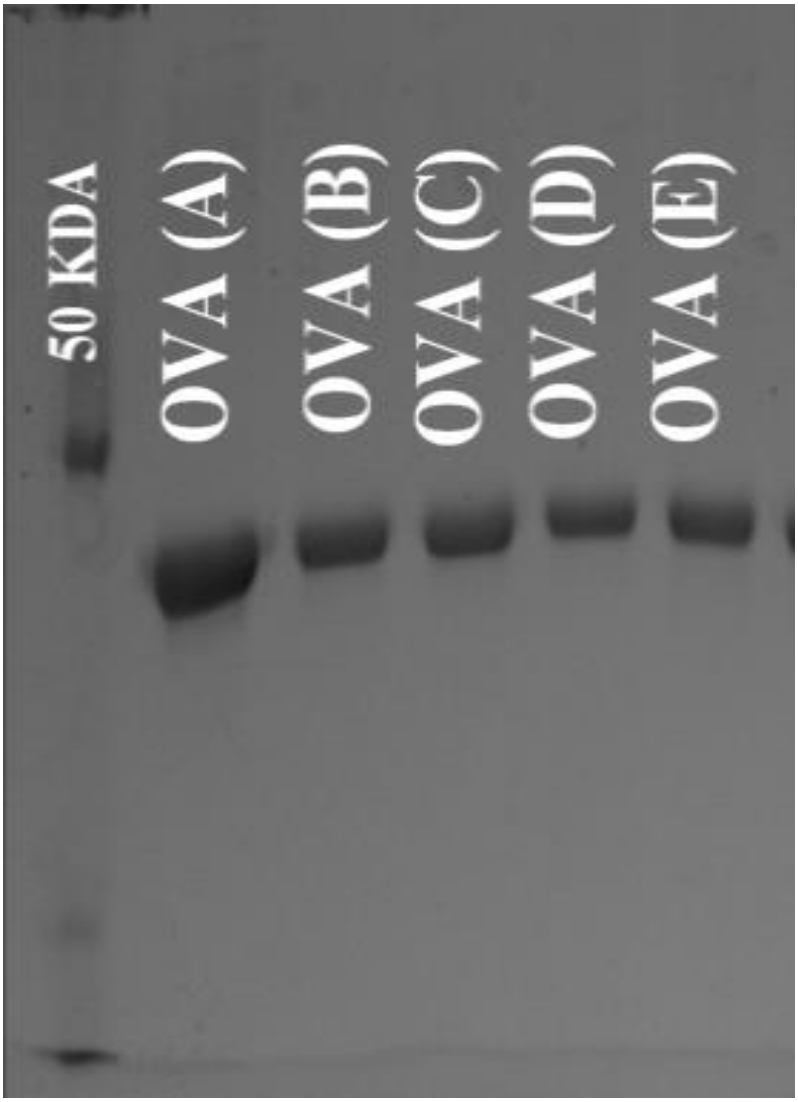

Figure 7

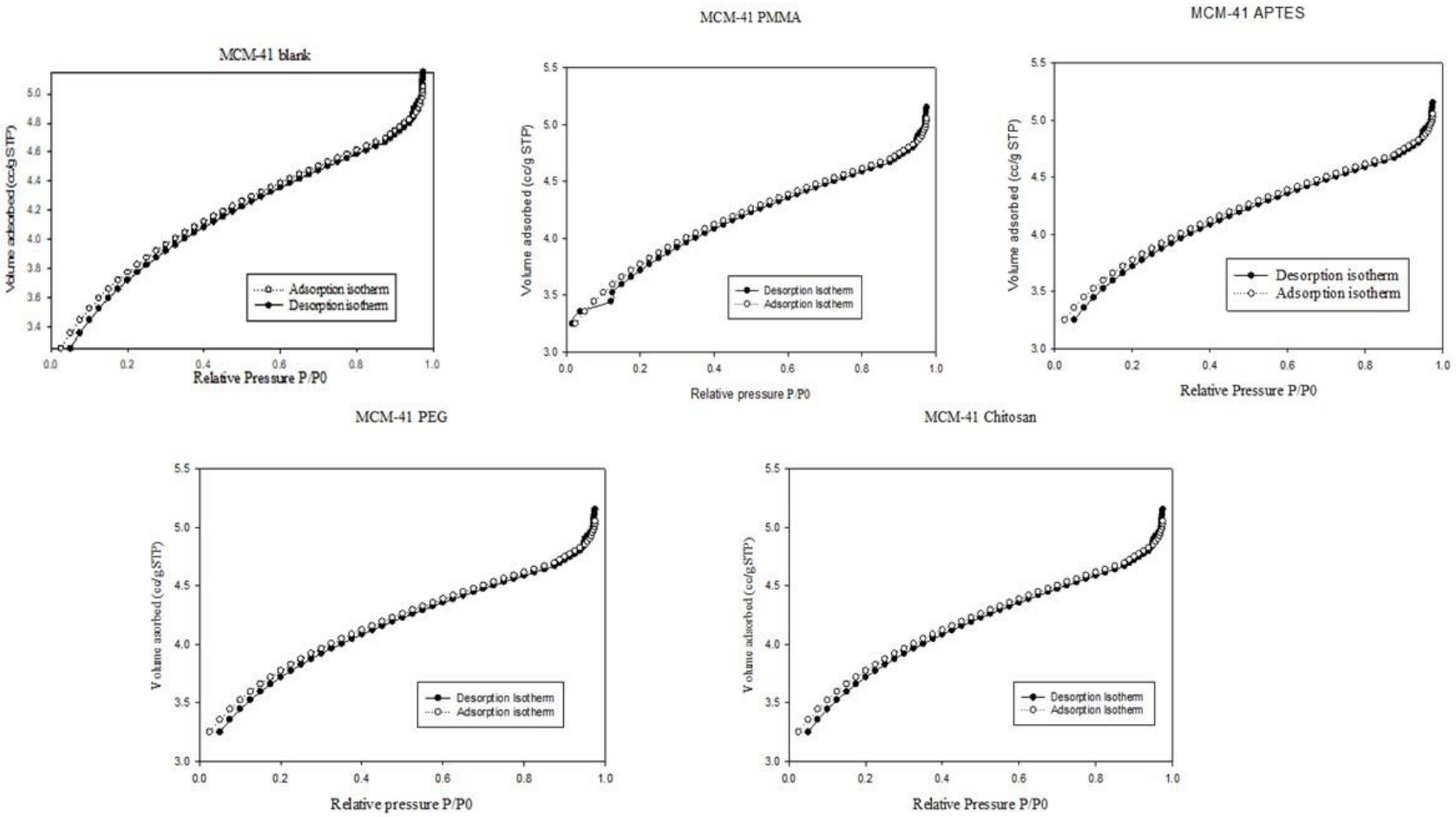

64

65 Figure 8